Crystal structure of the TSH receptor (TSHR) bound to a blocking-type TSHR autoantibody

Paul Sanders, Stuart Young, Jane Sanders, Katarzyna Kabelis, Stuart Baker, Andrew Sullivan, Michele Evans, Jill Clark, Jane Wilmot, Xiaoling Hu, Emma Roberts, Michael Powell, Ricardo Núñez Miguel, Jadwiga Furmaniak and **Bernard Rees Smith**

FIRS Laboratories, RSR Ltd, Parc Ty Glas, Llanishen, Cardiff CF14 5DU, UK

(Correspondence should be addressed to B Rees Smith; Email: firs@rsrltd.eclipse.co.uk)

Abstract

A complex of the TSH receptor extracellular domain (amino acids 22–260; TSHR260) bound to a blocking-type human monoclonal autoantibody (K1-70) was purified, crystallised and the structure solved at 1·9 Å resolution. K1-70 Fab binds to the concave surface of the TSHR leucine-rich domain (LRD) forming a large interface (2565 $Å^2$) with an extensive network of ionic, polar and hydrophobic interactions. Mutation of TSHR or K1-70 residues showing strong interactions in the solved structure influenced the activity of K1-70, indicating that the binding detail observed in the complex reflects interactions of K1-70 with intact, functionally active TSHR. Unbound K1-70 Fab was prepared and crystallised to 2·22 Å resolution. Virtually no movement was observed in the atoms of K1-70 residues on the binding interface compared with unbound K1-70, consistent with 'lock and key' binding. The binding arrangements in the TSHR260–K1-70 Fab complex are similar to previously observed for the TSHR260–M22 Fab complex; however, K1-70 clasps the concave surface of the TSHR LRD in approximately the opposite orientation (rotated 155°) to M22. The blocking autoantibody K1-70 binds more N-terminally on the TSHR concave surface than either the stimulating autoantibody M22 or the hormone TSH, and this may reflect its different functional activity. The structure of TSHR260 in the TSHR260–K1-70 and TSHR260–M22 complexes show a root mean square deviation on all C_α atoms of only 0·51 Å. These high-resolution crystal structures provide a foundation for developing new strategies to understand and control TSHR activation and the autoimmune response to the TSHR.

Journal of Molecular Endocrinology (2011) **46,** 81–99

Introduction

The TSH receptor (TSHR) is a major autoantigen in autoimmune thyroid disease, and TSHR autoantibodies with thyroid-stimulating (agonist) activity are responsible for the hyperthyroidism of Graves' disease (Rees Smith *et al.* 1988, 2007, Rapoport *et al.* 1998, Sanders *et al.* 1997). However, in rare cases, TSHR autoantibodies act as antagonists and prevent the TSHR-binding and stimulating activities of TSH and can cause hypothyroidism (Rees Smith *et al.* 1988, 2007, McKenzie & Zakarija 1992, Sanders *et al.* 1997, Rapoport *et al.* 1998). The availability of human monoclonal antibodies to the TSHR with the characteristics of patient serum autoantibodies has allowed major developments in our understanding of the TSHR–autoantibody interaction, and in the case of thyroid-stimulating autoantibodies, the crystal structure of a human monoclonal autoantibody (M22) in complex with the TSHR (amino acids 22–260; TSHR260) has been determined at 2·55 Å resolution (Sanders *et al.* 2007*a*).

Recently, we have isolated two new human monoclonal autoantibodies to the TSHR from a single sample of a patient's peripheral blood lymphocytes (Rees Smith *et al.* 2009, Evans *et al.* 2010). One monoclonal antibody is a powerful thyroid stimulator (K1-18), and the other (K1-70) blocks the stimulating activities of TSH and TSHR autoantibodies (including M22 and K1-18). We now describe the crystal structure of K1-70 Fab unbound (solved at 2·22 Å) and the crystal structure of K1-70 Fab bound to TSHR260 (solved at 1·9 Å). Using the information obtained from the crystal structures, we then carried out a molecular level analysis of the antigen-binding surfaces of K1-70 (antagonist) and M22 (agonist) Fabs as well as a detailed comparison of the interactions of K1-70 and M22 with the TSHR.

Materials and methods

Preparation of K1-70 Fab for crystallisation

K1-70 IgG was prepared from heterohybridoma culture supernatants using protein A affinity chromatography on MabSelect (GE Healthcare, Little Chalfont, UK) according to the manufacturer's instructions. The purified IgG was treated with mercuripapain

0952–5041/11/046–081
DOI: 10.1530/JME-10-0127
Online version via http://www.endocrinology-journals.org

(Sigma–Aldrich, Poole, UK) at an enzyme/protein (w/w) ratio of 1:200, EDTA at a final concentration of 2 mmol/l and L-cysteine at a final concentration of 1 mmol/l for 1 h at 37 °C. The reaction was terminated by the addition of 50 mmol/l iodoacetamide in 2 mol/l Tris–HCl (pH 8·3) for 30 min at room temperature. The digest was passed through a MabSelect column to separate any intact IgG or Fc from the Fab preparation. K1-70 Fab for crystallisation was concentrated to 15·5 mg/ml using iCON concentrators (20 ml, 9K MWCO; ThermoFisher Scientific, Cramlington, UK). The integrity of the K1-70 Fab was analysed by SDS-PAGE, size-exclusion HPLC on a TSK gel G3000 SW column (Tosoh, Sigma–Aldrich), and the ability of K1-70 Fab to inhibit TSH–biotin binding to the TSHR was tested as described previously (RSR Ltd, Cardiff, UK; Bolton *et al.* 1999).

X-ray diffraction and structure determination of K1-70 Fab

K1-70 Fab crystals were grown using the hanging drop vapour diffusion method with the structure screen 1 sparse matrix screen from Molecular Dimensions Ltd (Soham, UK). Condition 24 (30% PEG 400, 0·1 M sodium HEPES, 0·2 M magnesium chloride, pH 7·5) yielded single crystals suitable for X-ray diffraction data collection. A single crystal of dimensions 0·3×0·2 ×0·2 mm was flash cooled in liquid nitrogen. X-ray diffraction data collections were performed at cryogenic temperatures. The dataset was collected using a Rigaku-007HF generator and an R-Axis IV image plate detector, and was indexed, integrated and scaled using MOSFLM and SCALA (Biofocus, Saffron Walden, UK).

The structure of K1-70 Fab was determined by the molecular replacement method using the pdb coordinates of 1LIL (V_L and C_L domains), 2BOS (V_H domain) and 2EH7 (V_L domain). Molecular replacement was performed using the program PHASER, and the resulting model given ten cycles of atomic refinement with tight geometric weights using REFMAC5 (Collaborative Computational Project number 4[CCP4] 1994). Electron density maps calculated after initial refinement were examined using COOT (Emsley *et al.* 2010) and automatically corrected and rebuilt using BUCCANEER (CCP4 1994). The structural geometry of K1-70 Fab was checked using PROCHECK (Laskowski *et al.* 1993, CCP4 1994) and RAMPAGE (CCP4 1994). Electrostatic potential surfaces of the antigen-binding sites were generated using PYMOL (DeLano 2002).

Preparation of the TSHR260–K1-70 Fab complex

A TSHR260 construct (coding for amino acids (aa) 1–260 of the human TSHR [764aas]) was produced and expressed in insect cells using the baculovirus system as described previously (Sanders *et al.* 2007*a*). Purified K1-70 Fab was added to High Five insect cell cultures 96 h post infection to a final concentration of 2 μg/ml. Culture supernatants containing TSHR260–K1-70 Fab complex were harvested 120 h post infection by centrifugation at 500 ***g*** for 10 min. One tablet of complete protease inhibitors (Roche Diagnostics, Lewes, UK) was added per 200 ml supernatant, before storing at −70 °C until purification.

Purification of TSHR260–K1-70 Fab complex

Culture supernatant containing the TSHR260–K1-70 Fab complex was adjusted to pH 6·4 with 500 mmol/l NaH_2PO_4 and loaded onto 75 ml Streamline Direct HST-1 matrix in a Streamline 25 expanded bed chromatography system (GE Healthcare), washed in 100 mmol/l NaCl and 50 mmol/l Tris–HCl (buffer A) pH 6·0, and then in buffer A pH 6·5 and eluted in buffer A pH 8·5. The presence of the TSHR260–K1-70 Fab complex in the eluted fractions was confirmed by western blot analysis using a mouse monoclonal antibody (1 μg/ml) reactive with a TSHR epitope within amino acids 246–260 (TSHR MAb 18C5; Jeffreys *et al.* 2002).

The TSHR260–K1-70 Fab complex was further purified by affinity chromatography using a mouse monoclonal antibody (TSHR MAb 14C4; Jeffreys *et al.* 2002) that binds to a conformational epitope within amino acids 22–261 of the TSHR extracellular domain coupled to CNBr-activated sepharose-4B (Sigma–Aldrich). The dialysed complex was then further purified using nickel affinity chromatography on an Ni-NTA agarose column (Qiagen, Crawley, UK). The complex was eluted with 80 mmol/l imidazole, 100 mmol/l NaCl and 50 mmol/l Tris–HCl (pH 8·0), dialysed into 100 mmol/l NaCl, 50 mmol/l Tris–HCl (pH 8·0) and used to set up deglycosylation reactions.

Deglycosylation of the TSHR260–K1-70 Fab complex

The purified complex was deglycosylated using Endoglycosidase F3 (Sigma–Aldrich) at an enzyme-to-complex ratio of 152 mU of enzyme per mg of complex in 50 mmol/l sodium acetate buffer (pH 4·5) at 20 °C for 5 days. The deglycosylation reactions were then adjusted to pH 6·5 using 200 mmol/l Tris–HCl, run onto a cation exchange HPLC Bioassist S column (Tosoh) using an Akta (GE Healthcare) platform. The complex was eluted using a pH gradient from 6·5 to 9·0.

Eluted complex was further purified by size-exclusion chromatography. TSHR260–K1-70 Fab preparations were applied to a Superdex 200 XK-26 preparative column in 150 mmol/l NaCl and 10 mmol/l Tris–HCl (pH 7·6), and purified complex eluted from the

column was adjusted to 20 mmol/l Tris–HCl and 25 mmol/l NaCl, pH 7·6. The complex was concentrated using an iCON concentrator (7 ml 9K MWCO; ThermoFisher) followed by a MicroCon YM-10 concentrator (Millipore, Watford, UK) to a final concentration of 10 mg/ml.

X-ray diffraction and structure determination of TSHR260–K1-70 Fab

Crystals of TSHR260–K1-70 Fab complex were obtained in 96-well plates using the PEG/Ion HT screen from Hampton Research (Aliso Viejo, CA, USA). The best conditions were optimised further in 24-well plates using a range of PEG 3350 concentration from 16 to 26%, and the best crystals grew in 16% PEG 3350, 0·2 M sodium malonate, pH 5·0. A single crystal (dimensions 0·3×0·1 ×0·1 mm) was transferred to a solution containing 22% PEG 3350, 0·2 M sodium malonate, pH 5·0, and flash frozen in liquid nitrogen. The dataset was collected on a Rigaku-007HF generator and an R-Axis IV image plate detector, and was indexed, integrated and scaled using MOSFILM and SCALA (Biofocus).

The unbound K1-70 Fab crystal structure and the TSHR260 crystal structure (Sanders *et al.* 2007*a*) were used for molecular replacement using the programs PHASER and REFMAC5 (CCP4 1994). Structural geometry was checked using PROCHECK and RAMPAGE (CCP4 1994). Electrostatic potential surfaces were generated using PYMOL (DeLano 2002). The TSHR–K1-70 structure has been deposited in the Protein Data Bank with accession number 2XWT.

Preparation of recombinant K1-70 Fab

The K1-70 heavy-chain (HC) RT-PCR product and the light-chain (LC) RT-PCR product with 'C' terminal six histidine tags were cloned into the Immunozap H/L vector (Stratagene Europe, Amsterdam, The Netherlands) into XhoI and SpeI, and SacI and XbaI restriction sites respectively (Sanders *et al.* 2004). Specific 'forward' and 'reverse' primers were designed to change the K1-70 nucleotide sequence to code for the appropriate amino acid mutation (Sanders *et al.* 2007*b*). Amino acid mutations in the K1-70 Fab HC or LC sequence were introduced using the Qwikchange Mutagenesis Kit (Stratagene) following the manufacturer's instructions. The presence of the wild-type or mutated HC or LC was verified by sequence analysis (Source BioScience, Cambridge, UK).

Plasmid DNA containing the K1-70 HC and LC sequences was transformed into HB2151 cells (GE Healthcare), and expression of recombinant Fab was induced in the presence of 1 mmol/l isopropyl-β-D galactoside and 0·3 mol/l sucrose. Expression of recombinant Fab was verified using western blot analysis (Birk & Koepsell 1987) with an anti-human IgG (Fab specific) antibody (SAFC, Poole, UK). Fabs were dialysed into PBS containing 0·2 g/l sodium azide and stored at −70 °C.

Briefly, 4 l supernatant containing K1-70 recombinant Fab (K1-70 rFab) were adjusted to pH 6·0 with 500 mmol/l sodium dihydrogen phosphate (pH 4·0) and loaded onto a 75 ml Streamline TM Direct HST-1 column (GE Healthcare). K1-70 rFab was eluted with 0·3 mol/l NaCl and 10 mmol/l Tris–HCl (pH 8·5) and finally purified by chromatography on an Ni-NTA agarose column (Qiagen). The purity of the eluted rFab was >95% as assessed by SDS-PAGE (Laemmli 1970), and the concentration of the K1-70 rFab was calculated from the absorbance at 280 nm on the basis that 1 absorbance unit is equivalent to 0·7 mg/ml Fab.

Culture supernatants containing non-mutated (wild type; WT) or mutated K1-70 rFab were quantified using the Pierce Easy-Titer Human IgG (H+L) assay kit (ThermoFisher) against a standard curve of purified K1-70 rFab as per the manufacturer's instructions.

Inhibition of TSH–biotin binding to the TSHR by wild-type and mutated K1-70 rFabs

The ability of WT and mutated K1-70 rFabs to inhibit TSH–biotin binding to TSHR-coated ELISA plate wells was determined as described previously (RSR Ltd; Bolton *et al.* 1999). A calibration curve prepared from purified rK1-70 Fab was included in each assay.

Briefly, 75 µl culture supernatant containing either WT or mutated rFab were diluted in 50 mmol/l NaCl, 20 mmol/l Tris–HCl, pH 7·8, 1% Triton X-100 and 1 mg/ml BSA, and after addition of 75 µl start buffer incubated in TSHR-coated wells at room temperature for 2 h with shaking, the assay was carried out as per the kit instructions. Inhibition of TSH–biotin binding was calculated as follows:

$$100\times\left(1-\frac{\text{OD450 in the presence of test material}}{\text{OD450 in the presence of control material}}\right)$$

Inhibition of TSH-stimulated cyclic AMP production in CHO cells expressing the TSHR

The ability of WT K1-70 and mutated K1-70 rFabs to inhibit the production of intracellular cyclic AMP (cAMP) stimulated by porcine (p) TSH was analysed. In these experiments, CHO cells were seeded into 96-well plates (12 500–20 000 cells per well) and incubated for 48 h in DMEM containing 10% FCS. The DMEM was removed, and dilutions of WT and mutated K1-70 rFabs (0·001–1 µg/ml final

concentration) in cAMP assay buffer (NaCl-free Hank's Balanced Salt Solution containing 1 g/l glucose, 20 mmol/l HEPES, 222 mmol/l sucrose, 15 g/l BSA and 0·5 mmol/l 3-isobutyl-1-methylxanthine, pH 7·4) in the presence of 3 ng/ml pTSH were added, and cells were incubated at 37 °C in an atmosphere of 5% CO_2 in air for 1 h. After removal of test solutions, cells were lysed by the addition of 0·1 mol/l HCl, 1% Triton X-100, and the cAMP concentration in the lysates was determined using the Direct Cyclic AMP Correlate EIA kit (Assay Designs, Inc., Ann Arbor, MI, USA).

In a separate series of experiments, the effect of native K1-70 Fab on pTSH-mediated cAMP production was tested using Flp-In CHO cells expressing mutated TSHR as described previously (Sanders *et al.* 2006).

Binding of K1-70 to alkaline phosphatase-labelled TSHR260 (TSHR260-AP)

Briefly, 75 µl start buffer (Bolton *et al.* 1999) and 75 µl human monoclonal antibody diluted in a pool of healthy blood donor (HBD) sera were added to ELISA plate wells coated with the full-length detergent solubilised TSHR and incubated for 30 min at room temperature with shaking (500 shakes per minute). Then the well contents were aspirated, and the wells were washed three times with wash buffer (50 mmol/l NaCl, 20 mmol/l Tris, pH 7·8, 1% Triton X-100) followed by the addition of 100 µl TSHR260-AP (diluted in wash buffer containing 0·2 g/l $MgCl_2{\cdot}6H_2O$ and 2 g/l BSA; Rees Smith *et al.* 2009). After incubation for 30 min at room temperature with shaking (500 shakes per minute), the wells were emptied, washed three times followed by the addition of 100 µl *p*-nitrophenyl phosphate (pNpp) substrate (Europa Bioproducts Ltd, Ely, Cambridge UK), and the plate was incubated in the darkness for 45 min. The reaction was stopped by the addition of 50 µl of 1 mol/l NaOH, and the absorbance was read at 405 nm.

Results

Crystal structure of K1-70 Fab

The structure of K1-70 Fab was determined at 2·22 Å resolution with a R_{work} factor of 21·7% and a R_{free} factor of 26·4% (Supplementary Table 1, see section on supplementary data given at the end of this article). The asymmetric unit contains two complete Fab K1-70 molecules, Fab_A and Fab_B, that are not related by non-crystallographic symmetry due to differences in elbow angles ($Fab_A = 145{\cdot}5°$ and $Fab_B = 163{\cdot}1°$). The structure of K1-70 is that of a standard Fab fragment with no glycosylation. The distribution of CDRs making up the binding site is standard, with CDRs HC3 and LC3 having a central position, HC1 and LC1 positioned further out, and HC2 and LC2 on the periphery.

Disulphide bonds are present between LC residues 23 and 88, 134 and 194, and between HC residues 22 and 92 and 142 and 208. There are 158 hydrogen bonds within the LC and 177 hydrogen bonds within the HC residues. The accessible surface area (ASA) buried in the interface in the crystal structure is 1717 $Å^2$ for the LC and 1592 $Å^2$ for the HC residues. The structure of K1-70 lacks electron density of the side chains R94 (CDR3 LC) and R58 (CDR2 HC). After addition of these side chains, the ASAs were recalculated as 1722 $Å^2$ for the LC and 1607 $Å^2$ for the HC residues. There are 47 residues in the interface, and 40·4% of these residues are polar; this is similar to M22, which has 43 residues in the interface, and 41·9% are polar (Sanders *et al.* 2004).

The combining region of the K1-70 antigen-binding site (Fig. 1) is a highly irregular surface dominated by acidic patches on one side and basic patches on the other side. The acidic patches are centred on D27B (CDR1 LC), D50 (CDR2 LC), D92 (CDR3 LC), D31 (CDR1 HC), D54 and D56 (CDR2 HC) and D96 (CDR3 HC). The basic patches are centred on residues K53 and R54 (CDR2 LC), R94 (CDR3 LC), R58 (CDR2 HC) and R101 (CDR3 HC), and outside the variable domain region K66 LC creates a basic patch. The surface of K1-70 Fab also contains aromatic residues from both the variable regions and residues located close to them (14 residues in total; Fig. 1). The surface of the combining region contains a cavity at the centre surrounded mostly by aromatic residues and one charged residue D50 LC. Furthermore, the inside of the cavity is lined by aromatic residues.

In comparison, the surface of the thyroid-stimulating human monoclonal autoantibody (M22) antigen-binding site is also highly charged with acidic patches on one side and basic patches on the other side (Fig. 1; Sanders *et al.* 2004).

Crystal structure of the TSHR260–K1-70 Fab complex

The structure of the TSHR260–K1-70 Fab complex was solved to 1·9 Å resolution (Fig. 2A), and the crystallographic analysis is summarised in Supplementary Table 2, see section on supplementary data given at the end of this article.

The structure of TSHR260 solved from the TSHR260–K1-70 Fab complex is similar to that previously determined from the TSHR260–M22 Fab complex (2·55 Å resolution; Sanders *et al.* 2007*a*). A comparison of these two TSHR260 structures shows a root mean square deviation (rmsd) on all C_α atoms of only 0·51 Å, with the highest deviation of 2·42 Å found in the C_α atom of H248.

As shown in Fig. 2 and described previously (Sanders *et al.* 2007*a*), TSHR260 has the shape of a slightly curved helical tube constructed from leucine-rich repeat motifs. It has opposed concave and convex surfaces, with an eleven-stranded β-sheet located on the concave surface (ten parallel strands, one per repeat and an anti-parallel strand at the N-terminus). The inner surface of the tube is lined with hydrophobic residues. The concave surface of TSHR260 is formed from an untwisted β-sheet (Fig. 2A), and its convex surface presents eight small strands (two residues each) forming two 3-stranded β-sheets and one 2-stranded β-sheet (Fig. 2A). There are five glycosylation sites (N77, N99, N113, N177 and N198) located on the convex surface, and all are glycosylated, although the sugars are too disordered to model with confidence at position N113. The structure of TSHR260 shows a non-bonded cysteine at residue 176, which is located in the convex surface but with its side chain placed within the hydrophobic core preventing possible disulphide bonding.

The N-terminal cysteines (C31 and C41) in the TSHR sequence are disulphide bonded. The new structure of TSHR260 solved at 1·9 Å shows residues C24, S25, S26, P27, P28 and C29 (Fig. 2B), while there was no electron density for these residues in the TSHR260–M22 Fab complex solved at 2·55 Å (Sanders *et al.* 2007*a*). The new TSHR260 crystal structure provides therefore details of disulphide bonding arrangements at the TSHR N-terminus and shows disulphide bonds between the 1st and 2nd cysteines (C24 and C29) and between the 3rd and 4th cysteines (C31 and C41; Fig. 2B).

Interactions in the TSHR260–K1-70 Fab complex

K1-70 Fab binds to the concave surface of the TSHR260 and is positioned more N-terminally than the M22 Fab (Sanders *et al.* 2007*a*). Also, K1-70 Fab is bound at an approximate rotation of 155° on the TSHR260 with respect to the position of M22 Fab, and the orientation of the K1-70 and M22 Fab HCs and LCs are opposite (Fig. 3). A comparison of the structure of bound K1-70 Fab in the TSHR260–K1-70 Fab complex and the structure of unbound K1-70 Fab shows that the majority of the residues located on the binding surface of the antibody variable domains have almost identical positions (rmsd of all C_α atoms of the variable domains is 0·45 Å; Supplementary Figure 1, see section on supplementary data given at the end of this article). The highest deviation for a backbone C_α atom is 1·29 Å observed for LC G16. In addition, only six of the bound K1-70 Fab residue side chains deviate by more than 3 Å from their positions in unbound K1-70 Fab (LC residues V19, R54 and T80, and HC residues Q3, N76 and R101).

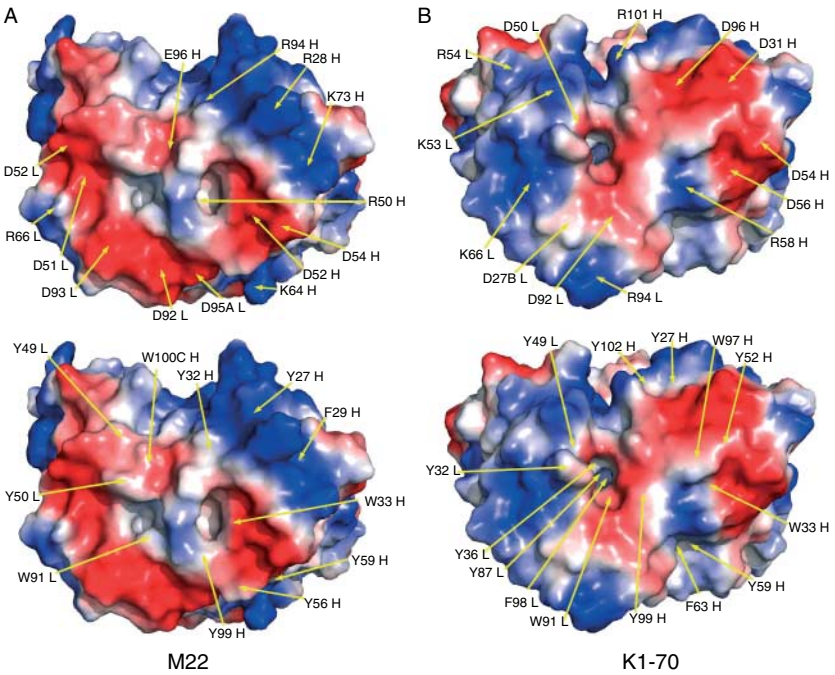

Figure 1 The electrostatic surface potentials (in Pymol; DeLano 2002) of the antigen-binding regions of (A) thyroid-stimulating monoclonal autoantibody (M22) and (B) TSH receptor-blocking monoclonal autoantibody (K1-70) showing the positions of charged residues (top figures) and the positions of aromatic residues (bottom figures). Acidic patches are shown in red, and basic patches are shown in blue.

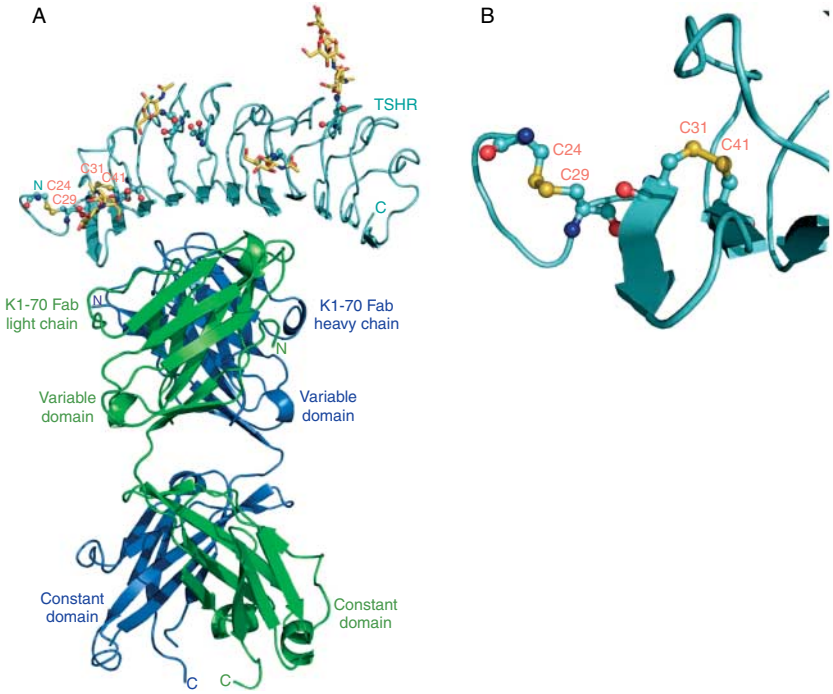

Figure 2 The complex of the TSH receptor leucine-rich repeat domain (TSHR LRD) and the human monoclonal autoantibody K1-70 Fab at 1·9 Å resolution. (A) Cartoon diagram of the complex structure. TSHR is in cyan, K1-70 light chain is in green, and K1-70 heavy chain is in blue. Disulphide-bonded cysteines are shown as ball and stick, disulphide bonds are in yellow, and cysteine residues are labelled in orange. The positions of amino (N)- and carboxy (C)-termini are indicated. (B) Disulphide bond arrangements in the N-terminal cap of the TSHR LRD in more detail. Cysteines are shown as ball and stick, disulphide bonds are shown in yellow, and cysteine residues are labelled in orange.

All of the glycosylation sites on the TSHR are distant from the K1-70 Fab-binding interface (Fig. 2).

A total of 2565 Å^2 of solvent ASA is buried in the K1-70–TSHR interface, 731 Å^2 in the interaction with K1-70 HC and 622 Å^2 in the interaction with the LC.

The interactions between TSHR260 and K1-70 Fab in the complex are a mixture of an extensive hydrogen bonding and salt bridge network (25 hydrogen bonds and salt bridges), 19 water-mediated hydrogen bonds, 11 polar interactions and 19 hydrophobic contacts (Table 1 and Fig. 4). There are 24 TSHR260 residues that form direct interactions with K1-70 Fab, and an additional four residues interact through water molecules. Furthermore, there are 12 K1-70 LC residues and 15 HC residues that interact directly with TSHR260 and an additional three LC residues that interact through water molecules. In particular, TSHR K58 is hydrogen bonded to three K1-70 residues (D31 HC, N32 HC and D96 HC), and the K1-70 residue D96 HC is hydrogen bonded to two TSHR residues (R38 and K58). In addition, some TSHR260 residues are involved in strong van der Waals interactions with K1-70, in particular TSHR R80 with an interaction surface of 101·5 Å^2 and TSHR F153 of 98·3 Å^2 (Table 2). K1-70 residues involved in van der Waals interactions with TSHR260 with large interacting surface areas include residues in both the HC and LC, for example W97 HC (117·3 Å^2) and R94 LC (97·9 Å^2; Table 2).

The high resolution (1·9 Å) of the TSHR260–K1-70 Fab complex and the availability of TSHR residues 24–29 in the structure (these were not present in the TSHR260–M22 complex (Sanders *et al.* 2007*a*)) provide new details of the structure of the TSHR N-terminus and reveal that the electrostatic surface potential is negatively charged (Fig. 4D). This is different from the assessment of the electrostatic potential distribution in the structure solved at 2·55 Å. The difference is due to disorder in this region of the TSHR260–M22 structure, while the TSHR260–K1-70 structure shows more detail.

The electrostatic surface potential of the TSHR260 concave surface and the K1-70 antigen-binding surface is polarised in terms of charge distribution. The surface distribution of charged residues on K1-70 is complementary to that of TSHR260, with the negatively charged surface of the TSHR260 interacting with the positively charged surface of K1-70 and the positively charged surface of TSHR260 interacting with the negatively charged surface of K1-70 (Fig. 4D).

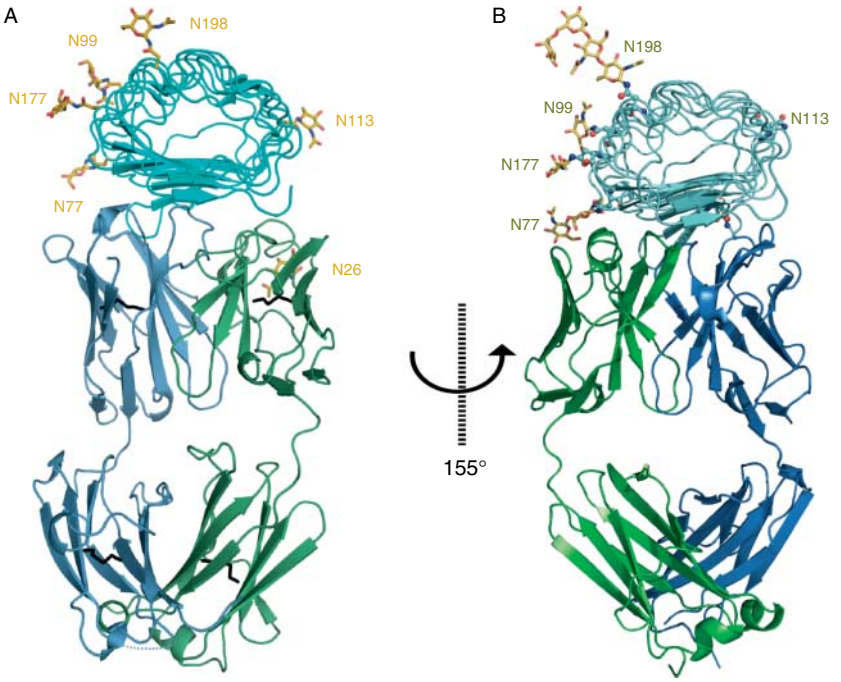

Figure 3 Comparison of the relative positions of the thyroid-stimulating autoantibody M22 and the TSH receptor (TSHR)-blocking monoclonal autoantibody (K1-70) on the TSH receptor leucine-rich repeat domain (TSHR LRD). (A) Crystal structure of TSHR260 in complex with thyroid-stimulating monoclonal autoantibody M22 Fab. TSHR is in cyan, M22 light chain (LC) is in green, and the M22 heavy chain (HC) is in blue. The N-terminal linked carbohydrates observed in the structure are shown in yellow, and carbohydrate bound asparagines residues are labelled. (B) Crystal structure of the TSHR260 in complex with the TSHR-blocking monoclonal autoantibody K1-70 Fab. The TSHR LRD is aligned in the same orientation as the TSHR LRD from the complex with M22 Fab (A). The relative positions of M22 and K1-70 Fabs bound to TSHR corresponds to a rotation about the TSHR vertical axis of ∼155°.

TSHR D203 is the last residue involved in charge–charge interactions in the TSHR260–K1-70 Fab complex interacting with K1-70 LC R94. The TSHR260 C-terminus is not involved in interactions with the K1-70 Fab (Fig. 2A). There are a number of electrostatic interactions in the TSHR260–K1-70 complex, and these are detailed in Table 3. TSHR R109 produces the strongest accumulated electrostatic interactions with K1-70, whereas K1-70 D31 HC and D50 LC produce the strongest accumulated electrostatic interactions with the TSHR (Table 3).

Effects of mutations in the TSHR and in K1-70 Fab

We analysed the effects of different amino acid mutations in the TSHR extracellular domain on the ability of K1-70 IgG to block pTSH-induced stimulation of cAMP production in CHO cells expressing the mutated TSHR (Table 4). Mutation of TSHR residues D43, R80, T104, H105, K129, F130, F134, D151, Q235, K250, E251, R255, T257 and W258 to alanine showed no significant effect (compared with wild-type TSHR) on stimulation of cAMP production by TSH or the TSH antagonist activity of K1-70 IgG. Furthermore, K1-70 binds strongly to TSHR260-AP in the bridge ELISA showing a similar dose-dependent response as the thyroid-stimulating monoclonal autoantibody M22. K1-70 and M22 IgG at 10 ng/ml gave an OD of 0·038 and 0·035 respectively (compared with 0·00 for HBD pool only), this increased to 0·993 and 1·045 at 500 ng/ml and a maximum of 1·416 and 1·532 at 100 μg/ml respectively. However, when full-length TSHR containing the R255D mutation was coated on the ELISA plate wells, K1-70 binding at 100 ng/ml was not significantly reduced (90% of WT TSHR binding), while M22 IgG binding was reduced to 13% of WT TSHR binding.

In the case of TSHR mutations that affected TSH stimulation of cAMP production, i.e. TSHR E107A, E157A, D160A, Y185A, D203A, Y206A, K209A and D232A, no significant effect on the TSH antagonist activity of K1-70 IgG was found. One mutation TSHR E178A caused a slight decrease in activity for both TSH stimulation of cAMP production and inhibition of TSH

Table 1 Interactions between TSHR260 and K1-70 Fab observed in the crystal structure of the complex

TSHR residue	TSHR atom	K1-70 residue[a]	K1-70 atom	Distance (Å)[b]
Hydrogen bonds and salt bridges[b]				
Asp36	OD2	Arg101 HC	NH1	2·80[c]
Asp36	OD1	Ser56 LC	N	2·99
Arg38	NE	Asp96 HC	OD1	2·74
Arg38	NH2	Asp96 HC	OD2	2·87[c]
Arg38	NH2	Tyr102 HC	OH	3·25
Lys42	NZ	Asp31 HC	OD1	2·88[c]
Gln55	OE1	Lys53 LC	NZ	2·88
Lys58	NZ	Asp31 HC	O	2·68
Lys58	NZ	Asn32 HC	OD1	2·99
Lys58	NZ	Asp96 HC	O	2·78
Arg80	NH1	Asp50 LC	OD2	2·78[c]
Arg80	NH2	Asp50 LC	OD1	2·98[c]
Try82	OH	Asn100 HC	ND2	2·92
Ser84	OG	Tyr52 HC	OH	2·96
Glu107	OE1	Trp97 HC	NE1	3·06
Arg109	NH1	Asp54 HC	OD1	2·85[c]
Arg109	NH1	Asp56 HC	OD2	3·02[c]
Arg109	NH2	Asp56 HC	OD2	3·23[c]
Lys129	NZ	Ser30 LC	O	2·91
Glu157	OE2	Arg58 HC	NH1	2·81[c]
Glu157	OE2	Arg58 HC	NH2	3·06[c]
Glu157	OE1	Tyr99 HC	OH	2·79
Thr181	OG1	Ser93 LC	O	3·04
Asp203	OD2	Arg94 LC	NE	3·03
Asp203	OD1	Arg94 LC	NH1	2·85[c]

TSHR residue	TSHR atom	Distance to water[b] (Å)	K1-70 residue[a]	K1-70 atom	Distance to water[b] (Å)	Water
Water-mediated hydrogen bonds						
Glu35	N	2·97	Tyr102 HC	OH	3·37	584
Asp36	O	2·73	Tyr49 LC	OH	2·80	218
Asp36	OD1	2·54	Arg54 LC	O	3·40	630
Gln55	OE1	2·80	Tyr49 LC	OH	2·80	218
Thr56	OG1	2·64	Asp96 HC	OD1	2·80	94
Thr56	OG1	2·64	Asn100 HC	OD1	2·74	94
Arg80	NE	2·95	Tyr99 HC	O	2·85	67
Arg80	NH2	3·19	Tyr99 HC	O	2·64	693
Lys102	O	2·52	Tyr32 LC	OH	2·76	497
Glu107	OE2	2·64	Asn98 HC	ND2	2·98	82
Asn110	ND2	2·66	Asp54 HC	OD1	2·91	124
Lys129	NZ	3·23	Gly29 LC	O	2·95	193
Lys129	NZ	2·67	Lys66 LC	NZ	2·81	581
Lys129	O	2·89	Ser93 LC	OG	2·53	191
Asp151	OD1	3·05	Lys66 LC	NZ	3·30	193
Phe153	O	2·74	Ser93 LC	OG	2·53	191
Lys183	NZ	2·56	Tyr99 HC	OH	2·75	343
Tyr206	OH	2·75	Arg94 LC	O	2·73	372
Tyr206	OH	2·97	Arg94 LC	O	3·20	458

TSHR	K1-70	TSHR	K1-70
Non-hydrogen bonding polar interactions[d]		Hydrophobic contacts[e]	
Asp36	Ser56 LC	Asp36	Pro55 LC
Arg38	Arg101 HC	Arg38	Arg101 HC
Arg80	Asn100 HC	Lys42	Asp31 HC
His105	Asn98 HC	Ile60	Asp31 HC
			Trp97 HC

(continued)

Table 1 *Continued*

TSHR	K1-70	TSHR	K1-70
Arg109	Arg58 HC	Glu61	Thr30 HC
Asn110	Asp54 HC	Tyr82	Trp97 HC
Lys129	Asn31 LC	Ser84	Trp97 HC
Asp151	Gly29 LC	Thr104	Tyr32 LC
	Ser30 LC	His105	Tyr99 HC
Phe153	Ser30 LC		
Lys183	Leu95 LC	Glu107	Trp97 HC
		Arg109	Trp33 HC
			Tyr52 HC
			Trp97 HC
		Phe130	Tyr99 HC
		Phe153	Ser27A LC
			Ser93 LC
			Arg94 LC
		Ile155	Ser93 LC

[a]LC, light chain and HC, heavy chain.
[b]Hydrogen bond distances are in the range of 2·3–3·4 Å.
[c]Denotes salt bridges.
[d]Polar contacts have distances between 3·4 and 4·0 Å.
[e]Carbon–carbon contacts are within 4·0 Å.

stimulation by K1-70 (<100–80%). In contrast, the TSHR mutations (K58A, I60A, E61A, Y82A, R109A and K183A) showed an absence or a decrease in TSH antagonist activity of K1-70, while TSH stimulation of cAMP production in the mutated TSHR was similar to that in the wild-type TSHR. Analysis of the interactions of these six residues in the TSHR–K1-70 complex showed that all six interacted with K1-70. In particular, K58, Y82 and R109 are involved in 7 out of the 25 hydrogen bonds and salt bridges present in the structure (Table 1), while K183 produces a water-mediated hydrogen bond with Y99 of the K1-70 HC. Also R109 and K183 are involved in non-hydrogen bonding polar interactions with R58 HC and L95 LC respectively, and I60, E61, Y82 and R109 form hydrophobic contacts (Table 1). R109 and K58 are involved in strong van der Waals interactions in the complex (Table 2) and form ion pairs with the K1-70 HC D54, D56 and D96 (Table 3).

In contrast, some TSHR amino acids that had no effect on the antagonist activity of K1-70 are involved in interactions within the complex. For example, TSHR R80 forms two salt bridges with K1-70 D50 LC, two water-mediated hydrogen bonds with Y99 HC, a non-hydrogen bonding polar interaction with N100 HC, a strong van der Waals interaction and two ion pair interactions with D50 LC. This shows that the absence of a detectable effect of a mutation in the TSHR on the actions of K1-70 on TSH stimulation does not necessarily indicate that there are no interactions involving this residue. In particular, a mutation may not show any effect if other interactions with the TSHR are not disrupted or are strong enough to compensate for the mutation (Lo Conte *et al.* 1999).

Wild-type and mutated K1-70 rFab preparations (N32A HC, R94D LC, W97A HC, Y99A HC and N100A HC) were expressed in *Escherichia coli*, and their activity was compared to the native K1-70 Fab produced by digestion of hybridoma K1-70 IgG. The activity of the K1-70 rFab showed a good agreement with the activity of the native Fab for inhibition of TSH–biotin binding and for inhibition of TSH-induced stimulation of cAMP production in CHO cells expressing the TSHR (Fig. 5A).

Western blotting showed that WT and mutated K1-70 rFab preparations contained <5% smaller cleavage products, and the results of the Easy-Titre (H+L) IgG assay showed that WT and mutated K1-70 rFabs were expressed at a similar level (3·7–6·0 μg/ml). We compared the activity of K1-70 rFab in *E. coli* culture supernatant (concentration of rFab measured in the Pierce Easy-Titre Human IgG assay kit) to the activity of purified K1-70 rFab (concentration measured by OD_{280}) using inhibition of TSH–biotin binding to the TSHR, and they were in good agreement (data not shown).

Mutation of K1-70 HC W97A and HC N100A greatly reduced the ability of K1-70 to inhibit TSH binding to TSHR-coated ELISA plate wells, i.e. 11·0 and 13·8% inhibition respectively at 0·1 μg/ml (compared with 93·6% by WT), and 17·4 and 37·8% respectively at 1 μg/ml (compared with 97·2% for WT; Fig. 5B). K1-70 mutations LC R94D, HC Y99A and HC N32A also had an effect giving 62·0, 55·2 and 71·7% inhibition of TSH binding at 0·1 μg/ml respectively compared with 93·6% in the case of WT (Fig. 5B).

The five K1-70 Fab mutations HC N100A, HC W97A, LC R94D, HC Y99A and HC N32A resulted in complete

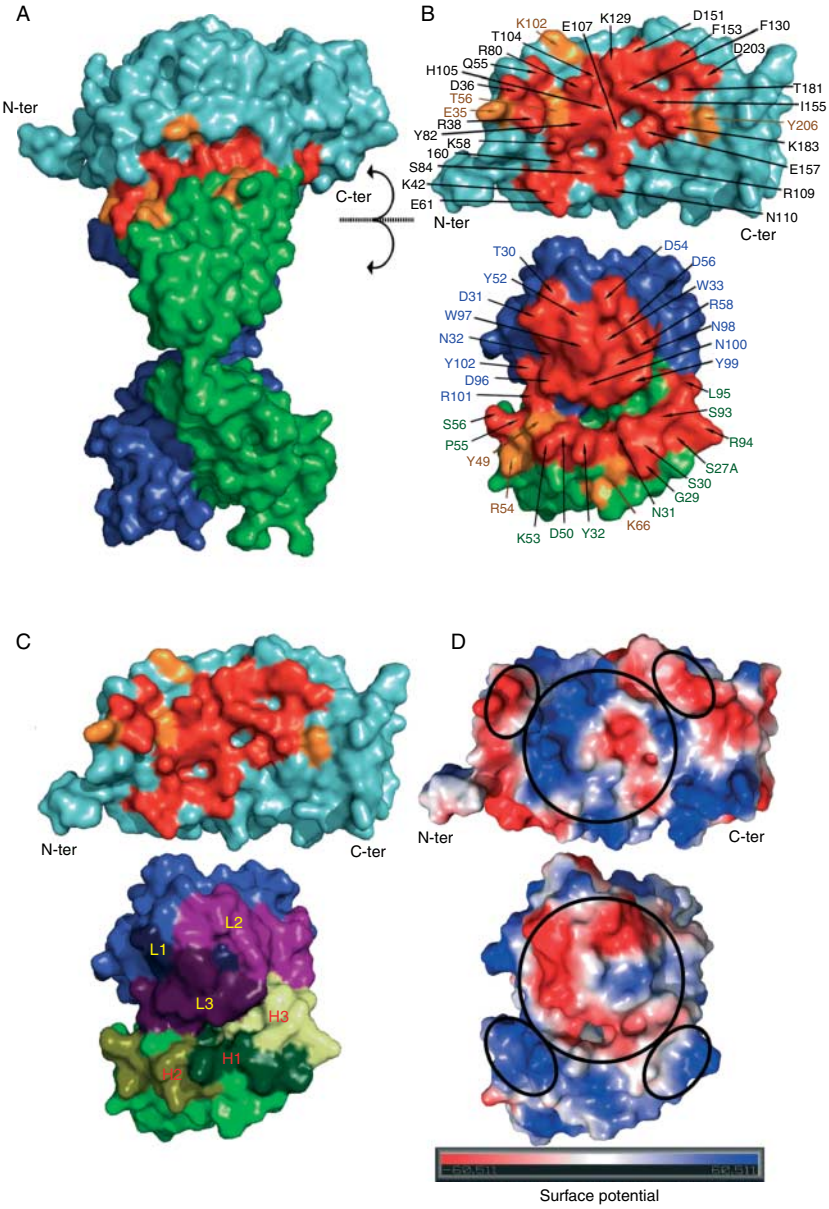

Figure 4 Interactions between K1-70 Fab and TSHR260. TSHR is shown in cyan, K1-70 heavy chain is in blue, and K1-70 light chain is in green. (A) The molecular surface of the TSHR260–K1-70 complex. TSHR residues are in cyan, K1-70 light chain is in green, and K1-70 heavy chain is in blue. (B) Opened up view of the interface area with residues of TSHR260 and K1-70 that are within 4·0 Å of each other highlighted in red and labelled, and those that interact only through water molecules are highlighted in orange and labelled. TSHR260 is shown in the top part of the figure and interacting residues are labelled. K1-70 is shown in the bottom part of the figure, the heavy chain residues are labelled in blue, and the light chain residues are labelled in green. (C) Hypervariable regions of K1-70 (bottom) are highlighted in different colours and labelled; TSHR (top) as in (B). (D) Electrostatic potential surface of TSHR260 (top) and K1-70 (bottom). Complementary potential surfaces between TSHR and K1-70 are enclosed in circles. The side chain of TSHR residue TSHR R250 is absent in the crystal structure and was modelled prior to generating the electrostatic surface potential of the TSHR LRD.

abolition of the ability to inhibit TSH-induced stimulation of cAMP production giving 0–1·9% inhibition at 1 μg/ml compared with 75·6% with WT K1-70 Fab (Fig. 5C). All five residues were observed to be involved in interactions with the TSHR in the crystal structure. Mutation of K1-70 HC W97 had the greatest effect with the ability of the mutant (1 μg/ml) to inhibit TSH binding to the receptor being <20% inhibition (compared with over 90% inhibition of TSH binding with wild-type K1-70) and with no effect on TSH-induced cAMP production being demonstrable (compared with over 70% blocking of TSH-induced cAMP stimulation with wild-type K1-70; Fig. 5B and C). In the crystal structure, K1-70 HC W97 is involved in a hydrogen bond with TSHR E107, hydrophobic contacts with I60, Y82, S84, E107 and R109, and has strong van der Waals interactions (Table 2). HC N100 forms a hydrogen bond with TSHR Y82, a water-mediated bond with T56 and a non-hydrogen bonding polar interaction with R80.

Comparison of TSHR–K1-70 Fab, TSHR–M22 Fab and TSHR–TSH complexes

Analysis of the TSHR260–K1-70 Fab, TSHR260–M22 Fab (Sanders *et al.* 2007*a*) crystal structures and the TSH–TSHR comparative model (Núñez Miguel *et al.* 2008) allowed a comparison of the binding arrangements within the complexes (Table 5).

As described previously, binding of the human thyroid-stimulating autoantibody M22 mimics the binding of TSH to the TSHR (Núñez Miguel *et al.* 2009). The M22 LC mimics the binding of the TSHβ chain as both interact with the 1st, 2nd, 4th, 6th, 7th, 8th, 9th and 10th repeats of TSHR260. The M22 HC mimics the binding of the TSHα chain and interacts with residues from the 1st through to the 7th repeat (Table 5). In contrast, the K1-70 LC interacts with the 1st through to the 8th repeat, and the HC with the 1st through to the 6th repeat. Consequently, K1-70 does not mimic either the interactions of TSH or M22 binding to the TSHR (Table 5).

A comparison of interactions in the interfaces of the three complexes demonstrates the increased number of stronger interactions with the TSHR (salt bridges and hydrogen bonds) in the case of K1-70 and M22 compared with the TSHR–TSH complex (25, 22 and 7 hydrogen bonds and salt bridges respectively; Table 5 and Fig. 6). The amino acid residues on the concave surface of the TSHR leucine-rich domain (LRD) that interact with TSH in a comparative model (Núñez Miguel *et al.* 2008), the thyroid-stimulating autoantibody M22 in the crystal structure (Sanders *et al.* 2007*a*) and the TSHR blocking autoantibody K1-70 in the crystal structure are detailed in Fig. 6. There are 24, 25 and 21 residues on the TSHR260 that interact with K1-70, M22 and TSH respectively (Fig. 6). Although the binding sites of the three ligands on the TSHR concave surface overlap extensively, the actual contact of amino acids differ. There are 16 amino acids that interact with both K1-70 and M22, 12 amino acids that interact with both K1-70 and TSH, and 13 amino acids that interact with both M22 and TSH. Furthermore, ten TSHR amino acids R38, K58, R80, H105, R109, N110, F130, F153, I155 and E157 interact with all three ligands (Fig. 6).

Table 2 Van der Waals interactions in the TSHR260–K1-70 complex. Van der Waals interactions were calculated as the accessible surface area (ASA) difference, for every amino acid, between the uncomplexed and complexed proteins. The ASA was calculated using the Lee and Richards algorithm developed by Richmond (Lee & Richards 1971, Richmond 1984)

(A) TSHR260 residues involved in strong (interaction surface area >60 Å^2) van der Waals interactions with K1-70 Fab	
Arg80	101·5 Å^2
Phe153	98·3 Å^2
Arg38	89·9 Å^2
Asp36	85·8 Å^2
Arg109	83·5 Å^2
Phe130	67·2 Å^2
Lys58	62·4 Å^2
Lys129	60·8 Å^2
(B) K1-70 Fab residues involved in strong (interaction surface area >60 Å^2) van der Waals interactions with TSHR260	
Trp97 HC	117·3 Å^2
Tyr99 HC	109·9 Å^2
Arg94 LC	97·9 Å^2
Tyr32 LC	81·9 Å^2
Asp31 HC	74·4 Å^2
Ser93 LC	74·2 Å^2
Ser30 LC	62·7 Å^2

Discussion

The availability of the crystal structure of K1-70 Fab (unbound) allowed us to compare the antigen-binding surfaces of this autoantibody with TSH-blocking (antagonist) activity and an autoantibody with thyroid-stimulating (agonist) activity (M22; Sanders *et al.* 2003, 2004). Both the K1-70 and M22 antigen-binding regions are rich in aromatic residues, and statistical analysis (Padlan 1990) has shown that tyrosines are three times more likely to be found in CDRs than in the frameworks of variable domains. The electrostatic surface potentials of both K1-70 and M22 TSHR-binding regions (Fig. 1) show highly irregular surfaces dominated by basic patches on one side and acidic patches on the other, although the distribution of the acidic and basic patches is virtually opposite for the two Fabs. In the case of M22, the negatively charged surface patches are formed predominantly by the LC residues, while on the

Table 3 Ion pair interactions in the TSH receptor (TSHR) LRD–K1-70 Fab complex. The interaction strengths shown for comparison, are in Newtons and are calculated using an in house program (ELECINT, R Nunez Miguel, unpublished) taking $\varepsilon = 1$ for electrostatic field calculation, and pH = 7·4 for the calculation of charges of side chain atoms of charged residues using the Henderson–Hasselbalch equation. Distances are between charged atoms

TSHR LRD	**K1-70 Fab**	**Distance** (strength)
By residue (interactions of strength $>10\times10^{-10}$ N)		
Asp36	Arg101 HC	2·80 Å ($14{\cdot}1\times10^{-10}$ N)
Arg38	Asp96 HC	2·87 Å ($15{\cdot}8\times10^{-10}$ N)
Lys42	Asp31 HC	2·88 Å ($22{\cdot}9\times10^{-10}$ N)
Arg80	Asp50 LC	2·77 Å ($22{\cdot}9\times10^{-10}$ N)
Arg109	Asp54 HC	2·85 Å ($12{\cdot}5\times10^{-10}$ N)
Arg109	Asp56 HC	3·02 Å ($14{\cdot}7\times10^{-10}$ N)
Glu157	Arg58 HC	2·81 Å ($20{\cdot}8\times10^{-10}$ N)
Asp203	Arg94 LC	2·85 Å ($16{\cdot}3\times10^{-10}$ N)
By atom (interactions of strength $>2{\cdot}5\times10^{-10}$ N)		
Asp36 OD2	Arg101 HC NH1	2·80 Å ($7{\cdot}4\times10^{-10}$ N)
	Arg101 HC NH2	3·84 Å ($3{\cdot}9\times10^{-10}$ N)
Arg38 NH2	Asp96 HC OD1	3·76 Å ($4{\cdot}1\times10^{-10}$ N)
	Asp96 HC OD2	2·87 Å ($7{\cdot}0\times10^{-10}$ N)
Lys42 NZ	Asp31 HC OD1	2·88 Å ($13{\cdot}8\times10^{-10}$ N)
	Asp31 HC OD2	3·56 Å ($9{\cdot}1\times10^{-10}$ N)
Lys58 NZ	Asp96 HC OD2	4·79 Å ($5{\cdot}0\times10^{-10}$ N)
Arg80 NH1	Asp50 LC OD1	3·42 Å ($4{\cdot}9\times10^{-10}$ N)
	Asp50 LC OD2	2·77 Å ($7{\cdot}5\times10^{-10}$ N)
Arg80 NH2	Asp50 LC OD1	2·98 Å ($6{\cdot}5\times10^{-10}$ N)
	Asp50 LC OD2	3·79 Å ($4{\cdot}0\times10^{-10}$ N)
Arg109 NH1	Asp54 HC OD1	2·85 Å ($7{\cdot}1\times10^{-10}$ N)
	Asp54 HC OD2	3·60 Å ($4{\cdot}4\times10^{-10}$ N)
	Asp56 HC OD2	3·02 Å ($6{\cdot}3\times10^{-10}$ N)
Arg109 NH2	Asp56 HC OD2	3·23 Å ($5{\cdot}5\times10^{-10}$ N)
Glu157 OE1	Arg58 HC NH1	3·70 Å ($4{\cdot}2\times10^{-10}$ N)
	Arg58 HC NH2	4·28 Å ($3{\cdot}1\times10^{-10}$ N)
Glu157 OE2	Arg58 HC NH1	2·81 Å ($7{\cdot}3\times10^{-10}$ N)
	Arg58 HC NH2	3·06 Å ($6{\cdot}2\times10^{-10}$ N)
Asp203 OD1	Arg94 LC NH1	2·85 Å ($7{\cdot}1\times10^{-10}$ N)
	Arg94 LC NH2	4·76 Å ($2{\cdot}5\times10^{-10}$ N)
Asp203 OD2	Arg94 LC NH1	3·71 Å ($4{\cdot}2\times10^{-10}$ N)

surface of K1-70, the negatively charged residues are from the HC. The positively charged residues on the surface of M22 are from the HC, whereas in the case of K1-70, they are from the LC (Fig. 1). These observations are consistent with the important role for charge–charge interactions for binding of TSHR autoantibodies to the TSHR observed experimentally (Rees Smith *et al.* 1988).

The crystal structure of the TSHR in complex with K1-70 that we describe provides details, at the molecular level, of how a human autoantibody that blocks TSH (and thyroid-stimulating autoantibody) stimulation interacts with the TSHR. Furthermore, the interactions of the TSHR with the blocking autoantibody (K1-70) can be compared with the interactions of the TSHR with the thyroid-stimulating autoantibody (M22; Sanders *et al.* 2007*a*,*b*).

A comparison of the TSHR260 structure when in complex with K1-70 or M22 shows an rmsd on all C_α atoms between the structures of only 0·51 Å confirming the original solved structure of the TSHR LRD (Sanders *et al.* 2007*a*). Furthermore, the conformation of the TSHR260 structure shows no significant change between the complex with the blocking monoclonal antibody K1-70 and the complex with the stimulating monoclonal antibody M22. This observation suggests that the first step in the process of TSHR activation by stimulating antibodies (such as M22), i.e. ligand binding, does not involve a direct conformational change of the TSHR LRD, and how the binding of M22 (or other TSHR-activating ligands) causes receptor activation is not clear at present. It may be that initial binding to the TSHR LRD induces changes in the hinge region between the LRD and transmembrane domain (TMD). Then this conformational change could cause activation of the TMD (Kleinau *et al.* 2008, Mizutori *et al.* 2008, Mueller *et al.* 2008). Crystal structures of the complete TSHR extracellular domain in complex with M22 and in complex with K1-70 should provide key insights into the mechanism of activation.

In the asymmetric unit of the crystals, there was only one complex consisting of one molecule of TSHR260

Table 4 Cyclic AMP production by TSH and blocking of TSH stimulation of cyclic AMP production by a human monoclonal autoantibody K1-70; effects in CHO cells transfected with mutated TSH receptor (TSHR)[a]

TSHR mutation	Stimulation of cyclic AMP production by TSH	Blocking of TSH-mediated stimulation of cyclic AMP production by K1-70 IgG
Wild type	+++++	+++++
Asp43 Ala	+++	+++++
Lys58 Ala	+++++	+
Ile60 Ala	+++++	++
Glu61 Ala	++++	+++
Arg80 Ala	+++++	+++++
Tyr82 Ala	+++++	+++
Thr104 Ala	+++++	+++++
His105 Ala	+++++	+++++
Glu107 Ala	+++	+++++
Arg109 Ala	+++++	+
Lys129 Ala	+++++	+++++
Phe130 Ala	+++++	+++++
Phe134 Ala	+++++	+++++
Asp151 Ala	+++++	+++++
Glu157 Ala	++	+++++
Aso160 Ala	+++	+++++
Glu178 Ala	++++	++++
Lys183 Ala	+++++	+++
Tyr185 Ala	++++	+++++
Asp203 Ala	++++	+++++
Tyr206 Ala	++++	+++++
Lys209 Ala	++++	+++++
Asp232 Ala	+++	+++++
Gln235 Ala	+++++	+++++
Lys250 Ala	+++++	+++++
Glu251 Ala	+++++	+++++
Arg255 Ala	+++++	+++++
Thr257 Ala	+++++	+++++
Trp258 Ala	+++++	+++++

[a]Relative effects of TSHR mutations were expressed as a percentage of activity observed with wild type: +++++, 100% wild-type activity; ++++, <100–80% wild-type activity; +++, <80–60% wild-type activity; ++, <60–40% wild-type activity; +, <40–20% wild-type activity.

bound to one molecule of K1-70 Fab. This was also the case in the TSHR260–M22 crystal structure (Sanders *et al.* 2007*a*), and consequently there was no evidence of dimer formation in either complex. In contrast, in the case of the FSHR–FSH complex crystal structure (solved at 2·9 Å; Fan & Hendrickson 2005), there were two complexes in the asymmetric unit. This difference could reflect differences in packing within the crystal, although FSHR–FSH complex dimerisation has been proposed (Fan & Hendrickson 2005).

The higher (1·9 Å) resolution of the TSHR260–K1-70 structure provided details of the disulphide bond arrangements at the N-terminus of the TSHR for the first time (Fig. 2B). Disulphide bonds are present between the 1st and 2nd cysteines (C24 and C29) and between the 3rd and 4th cysteines (C31 and C41). Thus, N-terminal cysteine disulphide bonding arrangements in the TSHR are different to that observed in the case of the FSHR crystal structure, where the 1st and 3rd cysteines (C18 and C25) and the 2nd and 4th cysteines (C23 and C32) are disulphide bonded (Fan & Hendrickson 2005). The TSHR has a three amino acid insertion between TSHR C31 and C41 when compared with the FSHR sequence, and consequently bonding between C29 and C41 of the TSHR would be entropically less favourable. Based on TSHR mutagenesis studies reported previously (Chen *et al.* 2001), it was proposed that C41 was paired to either C29 or C31, but our crystal structure now provides molecular level detail of the cysteine pairing at the N-terminus of the TSHR including C41 paired to C31.

In the crystal structure, K1-70 shows no interaction with the extreme N-terminus of the TSHR LRD, which contains the bonded cysteines. Analysis of the interaction of M22 with the TSHR (using the TSHR LRD structure from the complex solved at 1·9 Å) also showed that there were no M22 interactions involving the extreme N-terminal region of the TSHR LRD. These observations suggest that the TSHR region containing the four disulphide-bonded cysteines does not have a major role in TSHR autoantibody binding and most likely acts as a protective N-terminal cap aiding stability, preventing degradation and keeping the correct conformation of the receptor. This is not consistent with previous studies, which have concluded that the TSHR N-terminal region is part of a highly conformational epitope for thyroid-stimulating autoantibodies (Chen *et al.* 2001, Chazenbalk *et al.* 2004).

The crystal structure of the complex shows that the K1-70 Fab clasps the concave surface of the TSHR LRD in a similar way to M22 Fab but is in approximately the opposite orientation (i.e. rotated by ∼155° on the TSHR helical tube axis; Fig. 3). However, K1-70 binds more N-terminal on the TSHR interacting with an extensive surface of the receptor between amino acid D36 and D203, while the binding site of M22 extends further towards the C-terminus and spans the region between TSHR amino acids D36 and N256 (Fig. 3). The concave surface of the TSHR that interacts with K1-70 is extensive (ΔASA 2565·4 Å^2) and is greater than that typically observed for an antibody–antigen interface (Jones & Thornton 1996, Lo Conte *et al.* 1999). This observation together with the presence of a large number of hydrogen bonds, salt bridges and van der Waals interactions in the interface reflects the high binding affinity of K1-70 for the TSHR. Similar types and levels of interaction are observed for M22 (Sanders *et al.* 2007*a*). In contrast, there are only seven hydrogen bonds and salt bridges in the TSHR260–TSH complex (comparative model Núñez Miguel *et al.* 2008) compared with 25 and 22 in the complex of TSHR260 with K1-70 or M22 respectively, and this reflects the

differences in binding affinity of these three ligands to the TSHR.

Comparison of the structures of K1-70 Fab unbound and bound to the TSHR260 indicates that there is essentially no movement in the atoms of K1-70 residues upon binding to the TSHR, which is consistent with a 'lock and key' mode of binding (Supplementary Figure 1). This was also observed in the case of M22 binding to the TSHR (Sanders *et al.* 2007*a*), and consequently, loss of free energy through induction of a conformational change in either K1-70 or M22 does not occur during binding, and this is also consistent with the observed high affinity of the autoantibody–receptor interaction (McLachlan & Rapoport 1996, Sanders *et al.* 2003, 2004, 2008, Nakatake *et al.* 2006, Morganthaler *et al.* 2007, Thorpe & Brooks 2007, Rees Smith *et al.* 2009, Evans *et al.* 2010). In contrast to autoantibody binding to the TSHR, considerable conformational changes occur in FSH on binding to the FSH receptor (Fan & Hendrickson 2005).

Results from TSH binding and cAMP stimulation assays using mutated TSHR or K1-70 Fab provided experimental evidence confirming interactions observed in the crystal structure. Mutations of different TSHR residues that showed strong interactions in the structure influenced K1-70 activity, indicating that the binding arrangements in the complex reflect the interactions of K1-70 with intact, functionally active TSHR at least *in vitro*, and it is most likely that similar interactions take place when the TSHR and K1-70 combine *in vivo*.

However, due to the large interfaces of the interacting surfaces of all three ligands (K1-70, M22 and TSH; 2565, 2514 and 2533 Å^2 respectively) with the TSHR, mutation of some interacting residues may not show an effect on binding and/or biological activity (Lo Conte *et al.* 1999). For example, TSHR R80 forms several interactions with K1-70 in the complex, but mutation of this residue does not affect K1-70 activity. This is also the case for the mutation of TSHR E251 to alanine (Sanders *et al.* 2006, Chen *et al.* 2010), which interacts with TSH K44β in the TSH–TSHR comparative model (Núñez Miguel *et al.* 2008). The salt bridge formed between TSHR E251 and TSH K44β would not be formed in the case of TSHR E251A mutation; however, as this interaction is on the periphery of the interface, the mutation would be unlikely to affect TSH

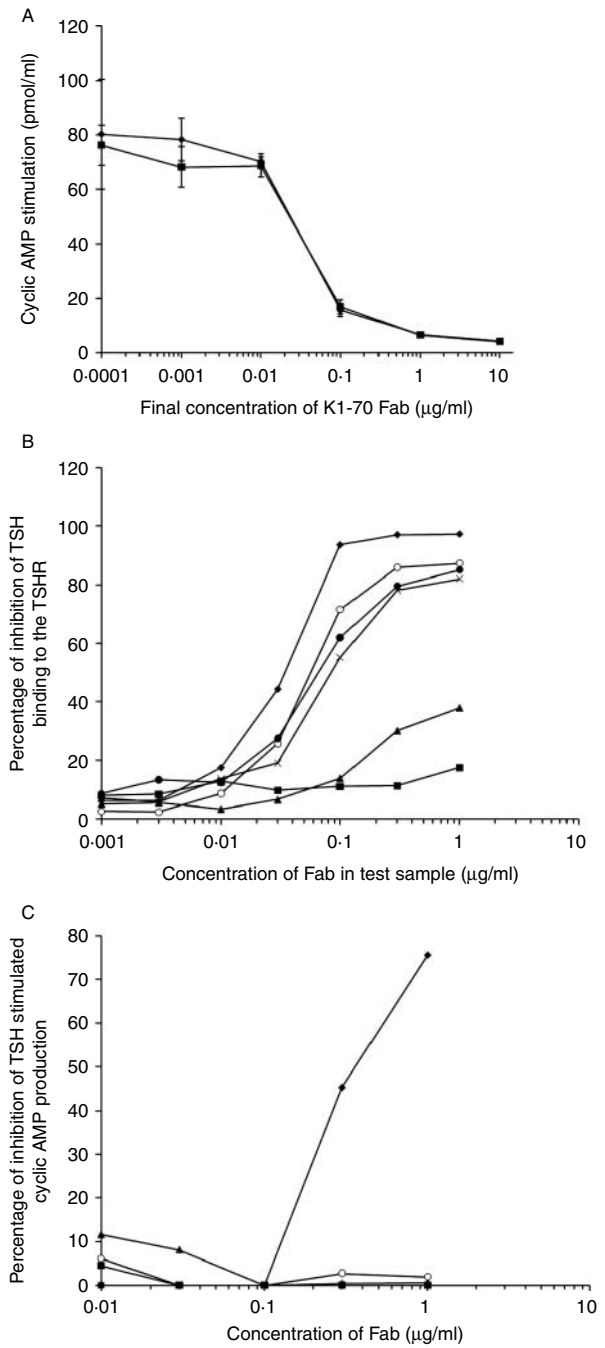

Figure 5 (A) Effects of K1-70 recombinant Fab (filled square)- and native hybridoma (filled diamond)-produced K1-70 Fab preparations on the inhibition of porcine TSH (pTSH) stimulation of cAMP in CHO cells expressing wild-type TSH receptor (TSHR). Final concentration of pTSH was 3 ng/ml and gave 76·5 ±7·2 pmol/ml cAMP production in the absence of K1-70 preparations. Mean of triplicate determinations. (B) Effects of wild-type and mutated K1-70 recombinant Fabs on the inhibition of TSH binding to TSHR coated onto ELISA plates. Test samples (75 μl) were added to 75 μl start buffer in each well. Wild type (filled diamond), W97A HC (filled square), N100A HC (filled triangle), Y99A HC (multiplication sign), N32A HC (open circle), R94D LC (filled circle). (C) Effects of wild-type and mutated K1-70 recombinant Fabs on the inhibition of TSH stimulation of cyclic AMP production. Final concentration of TSH was 3 ng/ml. Wild type (filled diamond), W97A HC (filled square), N100A HC (filled triangle), Y99A HC (multiplication sign), N32A HC (open circle), R94D LC (filled circle).

Table 5 Interactions between the TSH receptor (TSHR) and TSH, M22 and K1-70

Chain	N-terminus	1st	2nd	3rd	4th	5th	6th	7th	8th	9th	10th
(A) Number of residues from TSH (α and β chains), M22 (heavy and light chains) and K1-70 (heavy and light chains) that interact with residues of the TSH receptor (TSHR) leucine-rich repeats											
TSHα	–	1	1	6	9	6	8	2	–	–	–
TSHβ	–	1	3	–	4	–	3	1	4	1	3
M22 LC	–	1	1	–	3	–	3	2	7	2	6
M22 HC	–	4	2	4	4	7	7	3	–	–	–
K1-70 LC	–	3	1	2	1	3	5	3	1	–	–
K1-70 HC	–	6	5	4	8	2	2	–	–	–	–

Complex	Salt bridges	Hydrogen bonds	Ion pairs	Polar	Dipole-induced dipole	Hydrophobic
(B) Number and type of interactions in the interface of the TSHR260–K1-70 complex (crystal structure solved at 1·9 Å), TSHR260–M22 (crystal structure solved at 2·55 Å) and the TSHR–TSH complex (comparative model)						
K1-70–TSHR	11	14	8	11	48	19
M22–TSHR	8	14	10	17	36	14
TSH–TSHR	4	3	7	18	36	22

binding and stimulating activities (Sanders *et al.* 2006, Chen *et al.* 2010).

Mutation studies (Sanders *et al.* 2006) identified TSHR R255 as important for the activity of the stimulating autoantibody M22 and patient serum-stimulating autoantibodies. However, mutation of TSHR R255 did not affect the TSH antagonist (blocking) activity of K1-70 and has also been reported to be unimportant for the antagonist activity of patient serum autoantibodies (Sanders *et al.* 2006). Furthermore, TSHR R255A has no effect on the antagonist activities of the mouse MAb-B2 (Sanders *et al.* 2005, 2006) and the human autoantibody 5C9 (Sanders *et al.* 2008; both with TSH and TSHR autoantibody antagonist activity). In addition, a bridge-type ELISA using TSHR260-AP and TSHR containing R255D mutation can distinguish between the blocking-type monoclonal autoantibody K1-70, which binds to the mutated TSHR, and the stimulating-type monoclonal autoantibody M22, which shows drastically reduced binding compared with the WT TSHR. In the crystal structure, K1-70 Fab does not interact with TSHR R255, and this is in agreement with the experimental studies described in this study and reported previously (Sanders *et al.* 2006, Rees Smith *et al.* 2009). In contrast, TSHR C-terminal patches are involved in electrostatic interactions with thyroid-stimulating autoantibody M22, and R255 is the most C-terminal TSHR260 residue showing charge–charge interactions with M22 LC D60 (Sanders *et al.* 2007*a*).

The exact location of the binding sites for blocking autoantibodies and stimulating autoantibodies on the TSHR molecule has been controversial. Experimental evidence from our laboratory (Sanders *et al.* 1999, 2002, 2006) and other laboratories (Nagayama *et al.* 1991, Rapoport *et al.* 1998, Morganthaler *et al.* 2003, 2007) suggests that the epitopes for both types of autoantibodies overlap extensively. In contrast, other reports based on studies with TSHR chimeras concluded that the major binding sites for thyroid-stimulating autoantibodies were located at the N-terminus of the TSHR amino acids 9–165 (Tahara *et al.* 1991, 1997, Kosugi *et al.* 1993, Kim *et al.* 1996, 1997, Minich & Loos 2000, Kung *et al.* 2001, Minich *et al.* 2004), while the epitopes of blocking-type autoantibodies were more towards the TSHR C-terminus (aa 261–370; Tahara *et al.* 1997, Minich & Loos 2000, Kung *et al.* 2001). However, the binding arrangements observed in the crystal structure of the TSHR complexed with a blocking-type autoantibody (K1-70) and a stimulating-type autoantibody (M22) clearly show that the binding sites of the two antibodies overlap considerably with K1-70 forming strong interactions with TSHR260 (aa 22–260), even though the previously suggested important blocking antibody epitope (aa 261–370) (Tahara *et al.* 1997, Minich & Loos 2000, Kung *et al.* 2001, Loos *et al.* 2007) is missing entirely. Furthermore, both K1-70 and M22 bind strongly in ELISAs based on TSHR260 (Rees Smith *et al.* 2009). However, there has been one report (Schwarz-Lauer *et al.* 2002) in which the TSHR-blocking activity of one patient serum could not be absorbed by purified TSHR289 (aa 22–289), even though the blocking antibodies in a different serum and all the stimulating antibodies studied were absorbed. This could indicate that occasional patient autoantibodies with blocking activity might bind outside the TSHR260 region. However, in a detailed study of the interaction of over 50 patient serum TSHR autoantibodies with

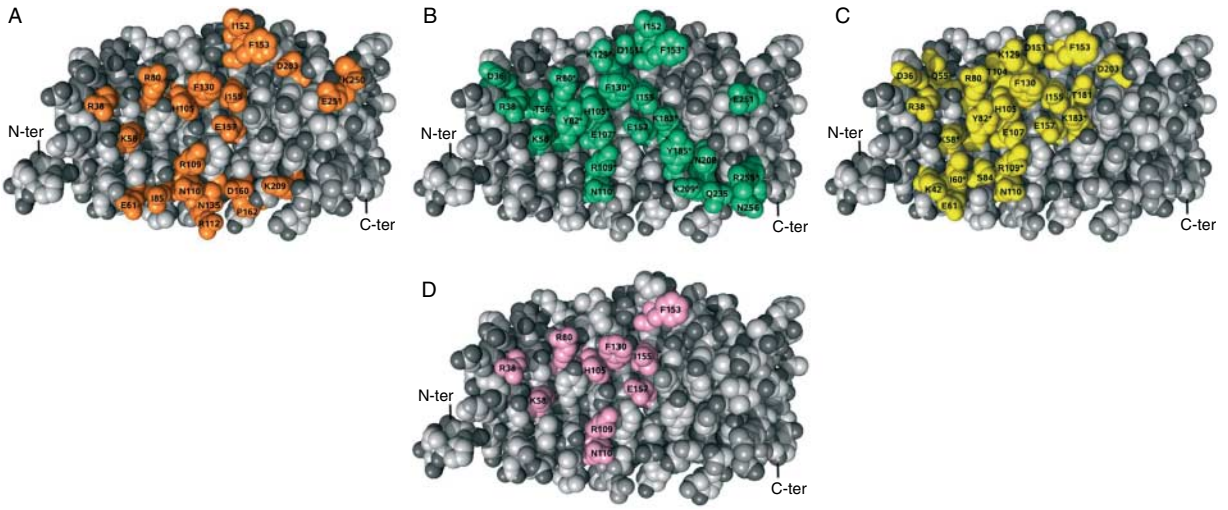

Figure 6 Space-fill representation of the TSH receptor leucine-rich repeat domain (TSHR LRD) interactive surface (based on the crystal structure of the TSHR260 in complex with K1-70 solved at 1·9 Å resolution). The N-terminus and the C-terminus are indicated. (A) TSHR residues that interact with TSH in our TSH–TSHR260 comparative model are shown in orange. (B) TSHR residues that interact with thyroid-stimulating autoantibody M22 in the TSHR260–M22 crystal structure are shown in green. (C) TSHR residues that interact with TSHR-blocking autoantibody K1-70 in the TSHR260–K1-70 crystal structure are shown in yellow. (D) TSHR residues that interact with all three ligands TSH, M22 and K1-70 are shown in pink.

TSHR260, all sera were found to interact strongly with this receptor preparation (Rees Smith *et al.* 2009). In addition, five sera in which blocking activity was established and five sera in which stimulating activity was established bound strongly to TSHR260.

A comparison of the interactions between the TSHR and the TSHR autoantibodies K1-70 and M22 and the hormone TSH was carried out using the respective crystal structures and a comparative model of the TSHR–TSH complex (Sanders *et al.* 2007*a*, Núñez Miguel *et al.* 2008). TSHR autoantibodies with different biological activities interact with the same region of the TSHR (the concave surface of the TSHR LRD) as TSH itself. Thus, the crystal structures provide further evidence for the overlap of the binding sites for TSHR autoantibodies and TSH observed in experimental studies (Rees Smith *et al.* 1988, Rapoport *et al.* 1998, Sanders *et al.* 1999, 2002, 2006, Morganthaler *et al.* 2003, 2007, Costagliola *et al.* 2004, Latif *et al.* 2009). Furthermore, the binding arrangements in the three complexes show important differences in the types of interactions present. In particular, interactions of K1-70 and M22 with the TSHR involve a greater number of strong interactions (hydrogen bonds and salt bridges) than in the case of TSH–TSHR binding. Also the interactions between FSH and FSHR in the crystal structure of the complex involve only six hydrogen bonds and salt bridges (Fan & Hendrickson 2005, Núñez Miguel *et al.* 2008). Thus, TSH or FSH binding to their respective receptors favours hydrophobic interactions, while binding of autoantibodies to the TSHR depends on stronger electrostatic interactions. The differences observed in the interactions in the complexes of the TSHR with TSH and with autoantibodies may reflect differences in how these complexes evolved. From an evolutionary perspective, it would be expected that hormone–receptor interactions have undergone evolutionary optimisations over a very long time that would include a trade-off between specificity of binding and effective biological function. In contrast, antibody–antigen interactions are subject to selection principally driven by binding affinity in addition to binding specificity (Jones & Thornton 1996, Lo Conte *et al.* 1999, Thorpe & Brooks 2007).

The crystal structures also showed that although M22 and K1-70 both bind to the concave surface of TSHR260 with considerable overlap, there are important differences. K1-70 interacts less with the C-terminus than TSH or M22. Furthermore, K1-70 HC and LC interactions with the TSHR LRD do not mimic the interactions of TSHα and TSHβ chains, while the interactions of M22 HC and LC do (Núñez Miguel *et al.* 2008). These arrangements most likely reflect the differences in the biological activity of the three ligands, and the observation of molecular mimicry between TSH and M22 (Núñez Miguel *et al.* 2008) but not between TSH and K1-70 provides a new perspective on the evolution of autoimmune responses in Graves' disease (Bork *et al.* 1993, Sanders *et al.* 2007*a*, Núñez Miguel *et al.* 2009).

Irrespective of the differences in the type of interactions and the regions on the TSHR LRD concave surface involved in binding to M22, K1-70 and TSH, all

three ligands form important interactions with the same ten TSHR residues (Fig. 6). This observation may be helpful in further understanding the molecular basis of binding between the TSHR and ligands with different biological activities and may lead to the development of new therapies for autoimmune diseases involving the TSHR.

Overall, the availability of high resolution crystal structures of the TSHR in complex with blocking-type and stimulating-type human monoclonal autoantibodies provides a foundation for developing new strategies to understand and control TSHR activation and the autoimmune response to the TSHR.

Supplementary data

This is linked to the online version of the paper at http://dx.doi.org/10.1530/JME-10-0127.

Declaration of interest

RSR Ltd is a developer of *in vitro* medical diagnostics including kits for measuring thyroid autoantibodies. All authors are employees of RSR Ltd.

Funding

The work was funded by RSR Ltd.

Acknowledgements

Some of the crystallisation trials, X-ray diffraction data collection and structure solving were carried out at Biofocus (Saffron Walden, UK) by Dr Philip Leonard.

References

Birk HW & Koepsell H 1987 Reaction of monoclonal antibodies with plasma membrane proteins after binding on nitrocellulose: renaturation of antigenic sites and reduction of non-specific antibody binding. *Analytical Biochemistry* **164** 12–22. (doi:10.1016/0003-2697(87)90360-5)

Bolton J, Sanders J, Oda Y, Chapman C, Konno R, Furmaniak J & Rees Smith B 1999 Measurement of thyroid-stimulating hormone receptor autoantibodies by ELISA. *Clinical Chemistry* **45** 2285–2287.

Bork P, Sander C & Valencia A 1993 Convergent evolution of similar enzymatic function on different protein folds: the hexokinase, ribokinase and galactokinase families of sugar kinases. *Protein Science* **2** 31–40. (doi:10.1002/pro.5560020104)

Chazenbalk GD, Latrofa F, McLachlan SM & Rapoport B 2004 Thyroid stimulation does not require antibodies with identical epitopes but does involve recognition of a critical conformation at the N terminus of the thyrotropin receptor A-subunit. *Journal of Clinical Endocrinology and Metabolism* **89** 1788–1793. (doi:10.1210/jc.2003-031554)

Chen CR, Tanaka K, Chazenbalk GD, McLachlan SM & Rapoport B 2001 A full biological response to autoantibodies in Graves' disease requires a disulfide-bond loop in the thyrotropin N-terminus homologous to a laminin EGF-like domain. *Journal of Biological Chemistry* **276** 14767–14772. (doi:10.1074/jbc.M008001200)

Chen CR, McLachlan SM & Rapoport B 2010 Thyrotropin (TSH) receptor residue E251 in the extracellular leucine-rich repeat domain is critical for linking TSH binding to receptor activation. *Endocrinology* **151** 1940–1947. (doi:10.1210/en.2009-1430)

Collaborative Computational project, number 4 1994 The CCP4 Suite: Programmes for protein Crystallography. *Acta Crystallographica* **D50** 760–763.

Costagliola S, Bonomi M, Morganthaler NG, Van Durme J, Panneels V, Refetoff S & Vassart G 2004 Delineation of the discontinuous-conformational epitope of a monoclonal antibody displaying full *in vitro* and *in vivo* thyrotropin activity. *Molecular Endocrinology* **18** 3020–3034. (doi:10.1210/me.2004-0231)

DeLano WL 2002 The Pymol molecular graphics system. DeLano Scientific, San Carlos, CA. http://pymol.sourceforge.net/.

Emsley P, Lohkamp B, Scott W & Cowtan K 2010 Features and developments of COOT. *Acta Crystallographica* **D66** 486–501. (doi:10.1107/S0907444910007493)

Evans M, Sanders J, Tagami T, Sanders P, Young S, Roberts E, Wilmot J, Hu X, Kabelis K, Clark J *et al.* 2010 Monoclonal autoantibodies to the TSH receptor, one with stimulating activity and one with blocking activity, obtained from the same blood sample. *Clinical Endocrinology* **73** 404–412. (doi:10.1111/j.1365-2265.2010.03831.x)

Fan QR & Hendrickson WA 2005 Structure of human follicle-stimulating hormone in complex with its receptor. *Nature* **433** 269–277. (doi:10.1038/nature03206)

Jeffreys J, Depraetere H, Sanders J, Oda Y, Evans M, Kiddie A, Richards T, Furmaniak J & Rees Smith B 2002 Characterization of the thyrotropin binding pocket. *Thyroid* **12** 1051–1061. (doi:10.1089/105072502321085144)

Jones S & Thornton JM 1996 Principles of protein–protein interactions. *PNAS* **93** 13–20. (doi:10.1073/pnas.93.1.13)

Kim WB, Cho BY, Park HY, Lee HK, Kohn LD, Tahara K & Koh C 1996 Epitopes for thyroid-stimulating antibodies in Graves' sera: a possible link of heterogeneity to differences in response to antithyroid drug treatment. *Journal of Clinical Endocrinology and Metabolism* **81** 1758–1767. (doi:10.1210/jc.81.5.1758)

Kim WB, Chung HK, Lee HK, Kohn LD, Tahara K & Cho BY 1997 Changes in epitopes for thyroid-stimulating antibodies in Graves' disease sera during treatment of hyperthyroidism: therapeutic implications. *Journal of Clinical Endocrinology and Metabolism* **82** 1953–1959. (doi:10.1210/jc.82.6.1953)

Kleinau G, Jaeschke H, Mueller S, Raaka BM, Neumann S, Paschke R & Krause G 2008 Evidence for cooperative signal triggering at the extracellular loops of the TSH receptor. *FASEB Journal* **22** 2798–2808. (doi:10.1096/fj.07-104711)

Kosugi S, Ban T & Kohn LD 1993 Identification of thyroid antibody-specific interaction sites in the N-terminal region of the thyrotropin receptor. *Molecular Endocrinology* **7** 114–130. (doi:10.1210/me.7.1.114)

Kung AWC, Lau KS & Kohn LD 2001 Epitope mapping of TSH receptor-blocking antibodies in Graves' disease that appear during pregnancy. *Journal of Clinical Endocrinology and Metabolism* **86** 3647–3653. (doi:10.1210/jc.86.8.3647)

Laemmli UK 1970 Cleavage of structural proteins during the assembly of the head of bacteriophage T5. *Nature* **227** 680–684. (doi:10.1038/227680a0)

Laskowski RA, MacArthur MW, Moss DS & Thornton JM 1993 PROCHECK – a program to check the stereochemical quality of protein structures. *Journal of Applied Crystallography* **26** 283–291. (doi:10.1107/S0021889892009944)

Latif R, Morshed SA, Zaidi M & Davies TF 2009 The thyroid stimulating hormone receptor: impact of thyroid-stimulating hormone and thyroid stimulating hormone receptor antibodies on multimerisation, cleavage, and signaling. *Endocrinology and Metabolism Clinics of North America* **38** 319–341. (doi:10.1016/j.ecl.2009.01.006)

Lee B & Richards FM 1971 The interpretation of protein structures: estimation of static accessibility. *Journal of Molecular Biology* **55** 379–400. (doi:10.1016/0022-2836(71)90324-X)

Lo Conte L, Chothia C & Janin J 1999 The atomic structure of protein–protein recognition sites. *Journal of Molecular Biology* **285** 2177–2198. (doi:10.1006/jmbi.1998.2439)

Loos U, Franz C, Minich WB & Büsselmann I 2007 Direct assay of TSH receptor autoantibodies causing Graves' disease correlates with the clinical diagnosis closer than assays based on TSH displacement. *Hormone Research* **68** (Supplement 3) 21–91.

McKenzie JM & Zakarija M 1992 Fetal and neonatal hyperthyroidism and hypothyroidism due to maternal TSH receptor antibodies. *Thyroid* **2** 155–159. (doi:10.1089/thy.1992.2.155)

McLachlan SM & Rapoport B 1996 Monoclonal, human autoantibodies to the TSH receptor – the holy grail and why are we looking for it? *Journal of Clinical Endocrinology and Metabolism* **81** 3152–3154. (doi:10.1210/jc.81.9.3152)

Minich WB & Loos U 2000 Detection of functionally different types of pathological autoantibodies against thyrotropin receptor in Graves' patients sera by luminescent immunoprecipitation analysis. *Experimental and Clinical Endocrinology and Diabetes* **108** 110–119. (doi:10.1055/s-2000-5804)

Minich WB, Lenzner C, Bergmann A & Morgenthaler NG 2004 A coated tube assay for the detection of blocking thyrotropin receptor autoantibodies. *Journal of Clinical Endocrinology and Metabolism* **89** 352–356. (doi:10.1210/jc.2003-030823)

Mizutori Y, Chen CR, McLachan SM & Rapoport B 2008 The thyrotropin receptor hinge region is not simply a scaffold for the leucine-rich domain but contributes to ligand binding and signal transduction. *Molecular Endocrinology* **22** 1171–1182. (doi:10.1210/me.2007-0407)

Morganthaler NG, Minich WB, Willnich M, Bogusch T, Hollidt JM, Weglohner W, Lenzner C & Bergmann A 2003 Affinity purification and diagnostic use of TSH receptor autoantibodies from human serum. *Molecular and Cellular Endocrinology* **212** 73–79. (doi:10.1016/j.mce.2003.09.018)

Morganthaler NG, Ho SC & Minich WB 2007 Stimulating and blocking thyroid stimulating hormone (TSH) receptor autoantibodies from patients with Graves' disease and autoimmune hypothyroidism have very similar concentration, TSH receptor affinity, and binding sites. *Journal of Clinical Endocrinology and Metabolism* **92** 1058–1065. (doi:10.1210/jc.2006-2213)

Mueller S, Kleinau G, Jaeschke H, Paschke R & Krause G 2008 Extended hormone binding site of the human thyroid stimulating hormone receptor. *Journal of Biological Chemistry* **283** 18048–18055. (doi:10.1074/jbc.M800449200)

Nagayama Y, Wadsworth HL, Russo D, Chazenbalk GD & Rapoport B 1991 Binding domains of stimulatory and inhibitory thyrotropin (TSH) receptor autoantibodies determined with chimeric TSH-lutropin/chorionic gonadotropin receptors. *Journal of Clinical Investigation* **88** 336–340. (doi:10.1172/JCI115297)

Nakatake N, Sanders J, Richards T, Burne P, Barrett C, Dal Pra C, Presotto F, Betterle C, Furmaniak J & Rees Smith B 2006 Estimation of serum TSH receptor autoantibody concentration and affinity. *Thyroid* **16** 1077–1084. (doi:10.1089/thy.2006.16.1077)

Núñez Miguel R, Sanders J, Chirgadze DY, Blundell TL, Furmaniak J & Rees Smith B 2008 FSH and TSH binding to their respective receptors: similarities, differences and implication for glycoprotein hormone specificity. *Journal of Molecular Endocrinology* **41** 145–164. (doi:10.1677/JME-08-0040)

Núñez Miguel R, Sanders J, Chirgadze DY, Furmaniak J & Rees Smith B 2009 Thyroid stimulating autoantibody M22 mimics TSH binding to the TSH receptor leucine rich domain: a comparative structural study of protein–protein interactions. *Journal of Molecular Endocrinology* **42** 381–395. (doi:10.1677/JME-08-0152)

Padlan EA 1990 On the nature of antibody combining sites. Unusual structural features that may confer on these sites an enhanced capacity for binding ligands. *Proteins* **7** 112–124. (doi:10.1002/prot.340070203)

Rapoport B, Chazenbalk GD, Jaume JC & McLachlan SM 1998 The thyrotropin (TSH) receptor: interaction with TSH and autoantibodies. *Endocrine Reviews* **19** 673–716. (doi:10.1210/er.19.6.673)

Rees Smith B, McLachlan SM & Furmaniak J 1988 Autoantibodies to the thyrotropin receptor. *Endocrine Reviews* **9** 106–121. (doi:10.1210/edrv-9-1-106)

Rees Smith B, Sanders J & Furmaniak J 2007 TSH receptor antibodies. *Thyroid* **17** 923–938. (doi:10.1089/thy.2007.0239)

Rees Smith B, Sanders J, Evans M, Tagami T & Furmaniak J 2009 TSH receptor–autoantibody interactions. *Hormone and Metabolic Research* **41** 448–455. (doi:10.1055/s-0029-1220913)

Richmond TJ 1984 Solvent accessible surface area excluded volume in proteins. Analytical equations for overlapping spheres and implications for the hydrophobic effect. *Journal of Molecular Biology* **178** 63–89. (doi:10.1016/0022-2836(84)90231-6)

Sanders J, Oda Y, Roberts SA, Maruyama M, Furmaniak J & Rees Smith B 1997 Understanding the thyrotropin receptor function–structure relationship. *Baillière's Clinical Endocrinology and Metabolism* **11** 451–479. (doi:10.1016/S0950-351X(97)80693-3)

Sanders J, Oda Y, Roberts S, Kiddie A, Richards T, Bolton J, McGrath V, Walters S, Jaskólski D, Furmaniak J *et al.* 1999 The interaction of TSH receptor autoantibodies with ^{125}I-labelled TSH receptor. *Journal of Clinical Endocrinology and Metabolism* **84** 3797–3802. (doi:10.1210/jc.84.10.3797)

Sanders J, Jeffreys J, Depraetere H, Richards T, Evans M, Kiddie A, Brereton K, Groenen M, Oda Y, Furmaniak J *et al.* 2002 Thyroid stimulating monoclonal antibodies. *Thyroid* **12** 1043–1050. (doi:10.1089/105072502321085135)

Sanders J, Evans M, Premawardhana LDKE, Depraetere H, Jeffreys J, Richards T, Furmaniak J & Rees Smith B 2003 Human monoclonal thyroid stimulating autoantibody. *Lancet* **362** 126–128. (doi:10.1016/S0140-6736(03)13866-4)

Sanders J, Jeffreys J, Depraetere H, Evans M, Richards T, Kiddie A, Brereton K, Premawardhana LD, Chirgadze DY, Núñez Miguel R *et al.* 2004 Characteristics of a human monoclonal autoantibody to the thyrotropin receptor: sequence structure and function. *Thyroid* **14** 560–570. (doi:10.1089/1050725041692918)

Sanders J, Allen F, Jeffreys J, Bolton J, Richards T, Depraetere H, Nakatake N, Evans M, Kiddie A, Premawardhana LDKE *et al.* 2005 Characteristics of a monoclonal antibody to the thyrotropin receptor that acts as a powerful thyroid-stimulating autoantibody antagonist. *Thyroid* **15** 672–682. (doi:10.1089/thy.2005.15.672)

Sanders J, Bolton J, Sanders P, Jeffreys J, Nakatake N, Richards T, Evans M, Kiddie A, Summerhayes S, Roberts E *et al.* 2006 Effects of TSH receptor mutations on binding and biological activity of monoclonal antibodies and TSH. *Thyroid* **16** 1195–1206. (doi:10.1089/thy.2006.16.1195)

Sanders J, Chirgadze DY, Sanders P, Baker S, Sullivan A, Bhardwaja A, Bolton J, Reeve M, Nakatake N, Evans M *et al.* 2007*a* Crystal structure of the TSH receptor in complex with a thyroid-stimulating autoantibody. *Thyroid* **17** 395–410. (doi:10.1089/thy.2007.0034)

Sanders J, Núñez Miguel R, Bolton J, Bhardwaja A, Sanders P, Nakatake N, Evans M, Furmaniak J & Rees Smith B 2007*b* Molecular interactions between the TSH receptor and a thyroid-stimulating monoclonal autoantibody. *Thyroid* **17** 699–706. (doi:10.1089/thy.2007.0041)

Sanders J, Evans M, Betterle C, Sanders P, Bhardwaja A, Young S, Roberts E, Wilmot J, Richards T, Kiddie A *et al.* 2008 A human monoclonal autoantibody to the thyrotropin receptor with thyroid-stimulating blocking activity. *Thyroid* **18** 735–746. (doi:10.1089/thy.2007.0327)

Schwarz-Lauer L, Chazenbalk GD, McLachlan SM, Ochi Y, Nagayama Y & Rapoport B 2002 Evidence for a simplified view of autoantibody interactions with the thyrotropin receptor. *Thyroid* **12** 115–120. (doi:10.1089/105072502753522347)

Tahara K, Ban T, Minegishi T & Kohn LD 1991 Immunoglobulins from Graves' disease patients interact with different sites on TSH receptor/LH-CG receptor chimeras than either TSH or

immunoglobulins from idiopathic myxedema patients. *Biochemical and Biophysical Research Communications* **179** 70–77. (doi:10.1016/0006-291X(91)91335-A)

Tahara K, Ishikawa N, Yamamoto K, Hirai A, Ito K, Tamura Y, Yoshida S, Saito Y & Kohn LD 1997 Epitopes for thyroid stimulating and thyroid blocking autoantibodies on the extracellular domain of the human thyrotropin receptor. *Thyroid* **7** 867–877. (doi:10.1089/thy.1997.7.867)

Thorpe IF & Brooks CL 2007 Molecular evolution of affinity and flexibility in the immune system. *PNAS* **104** 8821–8826. (doi:10.1073/pnas.0610064104)

Received in final form 8 November 2010
Accepted 1 December 2010
Made available online as an Accepted Preprint 19 January 2011